ACS NANO
Cite This: ACS Nano XXXX, XXX, XXX−XXX
www.acsnano.org

ARTICLE

Enhanced Performance of Ge Photodiodes *via* Monolithic Antireflection Texturing and α-Ge Self-Passivation by Inverse Metal-Assisted Chemical Etching

Munho Kim,[†] Soongyu Yi,[‡] Jeong Dong Kim,[†] Xin Yin,[§] Jun Li,[§] Jihye Bong,[‡] Dong Liu,[‡] Shih-Chia Liu,[∥] Alexander Kvit,[⊥] Weidong Zhou,[∥] Xudong Wang,[§] Zongfu Yu,[‡] Zhenqiang Ma,[‡] and Xiuling Li*[,†]

[†]Department of Electrical and Computer Engineering and Micro and Nanotechnology Laboratory, Materials Research Laboratory, University of Illinois at Urbana−Champaign, Urbana, Illinois 61801, United States,
[‡]Department of Electrical and Computer Engineering, University of Wisconsin at Madison, Madison, Wisconsin 53706, United States,
[§]Department of Material and Science Engineering, University of Wisconsin at Madison, Madison, Wisconsin 53706, United States,
[∥]Department of Electrical Engineering, University of Texas at Arlington, Arlington, Texas 76019, United States,
[⊥]Materials Science Center, University of Wisconsin at Madison, Madison, Wisconsin 53706, United States

Supporting Information

ABSTRACT: **Surface antireflection micro and nanostructures, normally formed by conventional reactive ion etching, offer advantages in photovoltaic and optoelectronic applications, including wider spectral wavelength ranges and acceptance angles. One challenge in incorporating these structures into devices is that optimal optical properties do not always translate into electrical performance due to surface damage, which significantly increases surface recombination. Here, we present a simple approach for fabricating antireflection structures, with self-passivated amorphous Ge (α-Ge) surfaces, on single crystalline Ge (c-Ge) surface using the inverse metal-assisted chemical etching technology (I-MacEtch). Vertical Schottky Ge photodiodes fabricated with surface structures involving arrays of pyramids or periodic nano-indentations show clear improvements not only in responsivity, due to enhanced optical absorption, but also in dark current. The dark current reduction is attributed to the Schottky barrier height increase and self-passivation effect of the i-MacEtch induced α-Ge layer formed on top of the c-Ge surface. The results demonstrated in this work show that MacEtch can be a viable technology for advanced light trapping and surface engineering in Ge and other semiconductor based optoelectronic devices.**

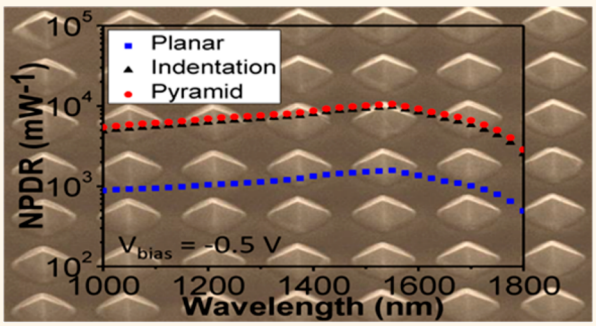

KEYWORDS: *metal-assisted chemical etching, germanium, photodiodes, surface texture, light trapping, antireflection coating*

Surface reflection is a phenomenon which occurs due to the refractive index difference between air and surfaces. It is one of the major limiting factors of light absorption efficiency in photovoltaic and optoelectronic devices. There have been considerable interests and activities in light trapping management of various semiconductor material surfaces.[1−3] Coating of antireflection (AR) layers can reduce the surface reflection, but this is only valid for a certain optical bandwidth and limited angular range. Direct formation of AR microstructures on the surface is proven to be effective to reduce reflections while minimizing the problems associated with traditional AR coatings. In recent years, advanced light trapping management using various types of AR microstructures has regained much attention. For instance, black-Si (b-Si) has been successfully exploited to improve performances of solar cells and photodiodes.[4,5] It is noted that b-Si has some disadvantages such as surface recombination due to a higher surface area. This issue has been addressed by using a conformal coating of a passivation layer by atomic layer deposition (ALD).[6] Similarly,

Received: March 11, 2018
Accepted: May 30, 2018
Published: May 30, 2018

ACS Publications © XXXX American Chemical Society

DOI: 10.1021/acsnano.8b01848
ACS Nano XXXX, XXX, XXX−XXX

numerous studies on AR microstructures on Ge have been reported.[7−9] However, there are few reports on Ge optoelectronic and photovoltaic devices using the AR microstructures,[10,11] probably because conventional reactive ion etching (RIE) used to create AR microstructures on Ge could induce significant damage in Ge.

Metal-assisted chemical etching (MacEtch or MaCE) is an alternative yet damage-free method to produce various types of micro and nanostructures.[12−14] The typical MacEtch process involves catalysts composed of noble metals (Au, Pt, Ag, *etc.*) and a chemical solution of an acid and an oxidant to selectively etch semiconductor surfaces. Because MacEtch is fundamentally a wet etch which does not involve high energy ions, it can eliminate unrepairable surface damages that can significantly degrade device performance.[15,16] Therefore, this emerging etching technique has been studied to create surface texturing for optoelectronic and photonic applications. However, the MacEtch enabled nanostructures have been mainly formed on Si and a few III−V compounds.[17,18] Lu *et al.*[10] reported MacEtch produced Ge nanoneedles combined with plasmonic enhancement for photodiode applications. Lee *et al.*[11] demonstrated MacEtch of Ge surface by diluted hydrogen peroxide (H_2O_2) in the absence of hydrofluoric acid (HF) catalyzed by randomly dispersed Ag nanoparticles, which led to the improvement of solar cell efficiency. Note that the MacEtch solution used in both of these studies[10,11] contained H_2O_2, which etches Ge without the presence of metal catalysts.

In this work, we present an inverse-MacEtch (I-MacEtch) approach to create two types of periodic surface texturing, pyramid and nano-indentation arrays on Ge surfaces. Photodiodes built on the MacEtch-textured Ge surfaces achieved significant improvements in both dark current and spectral responsivity compared to those made on the planar counterpart. This demonstration shows unambiguously that MacEtch can be a viable technology option to enhance performance of Ge-based optoelectronic devices. By analyzing the mechanism for these performance enhancements, understanding of the Ge i-MacEtch phenomenon, particularly the formation of an amorphous layer underneath the metal, is also provided.

RESULTS AND DISCUSSION

Formation of Textured Surface Structures. Figure 1a shows a tilted SEM image of an ordered array of pyramids on a Ge (100) surface produced by i-MacEtch using a Au catalyst dot pattern (25 nm thick) in a mixture of HF (0.56 M), DI water (1.1 M), and potassium permanganate ($KMnO_4$) (0.32 mM) for 90 min. Figure 1b shows schematic drawing of the patterned Au dot array and the illustration of the formation mechanism of the pyramids. Diameter and spacing of the patterns dots in the array are 5 and 2 μm, respectively. Inset in Figure 1a shows a zoomed-in SEM image of a single pyramid, with the bottom width being 4.2 μm and height being 0.94 μm. Scale bar in the inset is 1 μm. The size and shape of the pyramids are very uniform across the entire sample (5 × 5 mm^2). These pyramids are centered at the middle of the Au catalyst dots, indicating that Ge outside the metal catalyst area was etched first *via* i-MacEtch.[16,19] The three steps in the pyramid formation process are labeled as (ii), (iii), and (iv) in Figure 1b, which correspond to hole diffusion to the off-metal area, Ge removal, and Au lift-off after etching. In contrast to i-MacEtch of InP[19] which produced fins with vertical sidewalls underneath the catalyst metal, the i-MacEtch of Ge results in pyramids with four distinctive facets. The crystal orientation of

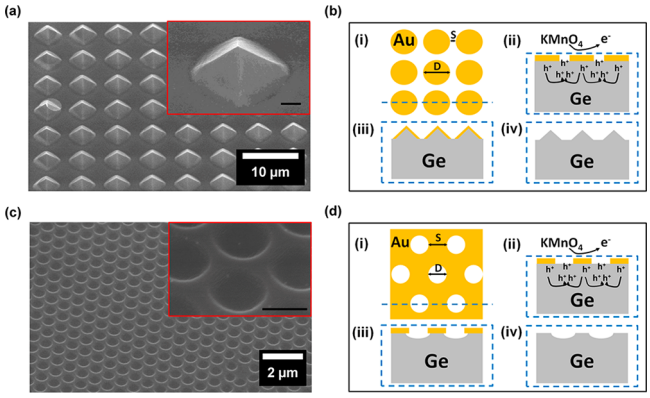

Figure 1. (a) Tilted SEM image of an array of MacEtched pyramids. Inset shows a zoomed-in image of the pyramid structure with a scale bar of 1 μm. (b) Schematic drawing of Au metal catalyst dot pattern and illustration of the formation mechanism of the Ge pyramids: (i) Au dot array with a diameter (D) of 5 μm and a spacing (S) of 2 μm, used to produce pyramid shaped Ge structures. (ii) Generation of holes (h^+) by reduction of $KMnO_4$ at catalyst and diffusion into off-metal area due to limited mass transport. (iii) Removal of Ge around and underneath the metal catalyst area *via* local oxidation and etching, leaving pyramid structures. (iv) Metal lift off after the MacEtch process. (c) Tilted SEM image of an array of nano-indentation structures. Inset shows a zoomed-in image of the nano-indentation structure with a scale bar of 500 nm. (d) Schematic drawing of Au metal catalyst mesh pattern (D = S = 400 nm) and illustration of the formation mechanism of the nano-indentation: (i) Au mesh pattern with a hole diameter and spacing of 400 nm, used to produce indentation shaped Ge structures. (ii) Generation of holes (h^+) by reduction of $KMnO_4$ at catalyst and diffusion into off-metal area due to limited mass transport. (iii) Removal of Ge at off-metal area *via* local oxidation and etching, leaving nano-indentation structures. (iv) Metal lift off after the MacEtch process.

the four facets is identified as (111), based on the measured angle (54.7°) with respect to the (100) substrate. Because the etch rate in <111> direction is the slowest on a (100) substrate for Ge, we attribute the facet formation to i-MacEtch induced chemical etching.[19,20] Table S1 summarizes hole mobility and hole diffusion coefficient of various semiconductor materials. Compared to silicon and other semiconductors, the high mobility and diffusion coefficient of holes in Ge indicate a higher chance of hole diffusion outside of the Au−Ge interface under the limited mass transport etching condition. To show how far the diffused holes can reach, Ge samples with 100 × 100 μm^2 size Au squares (thickness: 25 nm) were MacEtched by the same solution used for pyramid (see Figure S1). It is clearly observed that Ge close to the square begins to etch and the etched region gets larger with increasing etching time. It is worth mentioning that the backside of Ge was not protected during etching. We did not observe etching on the backside after being etched up to 90 min. We note that the transport length of holes (see Figure S1) is smaller than thickness of Ge (~550 μm). We believe that holes were consumed on the front before having time to diffuse to the backside for the duration of the etching. It should also be noted that the backside of the sample was thoroughly cleaned by spraying acetone to prevent any backside etching due to metal contaminants. SEM images of the pyramids during MacEtch are also provided in the Supporting Information (see Figure S2).

By the same mechanism, Figure 1c presents another demonstration of Ge i-MacEtch for periodically indented

DOI: 10.1021/acsnano.8b01848
ACS Nano XXXX, XXX, XXX−XXX

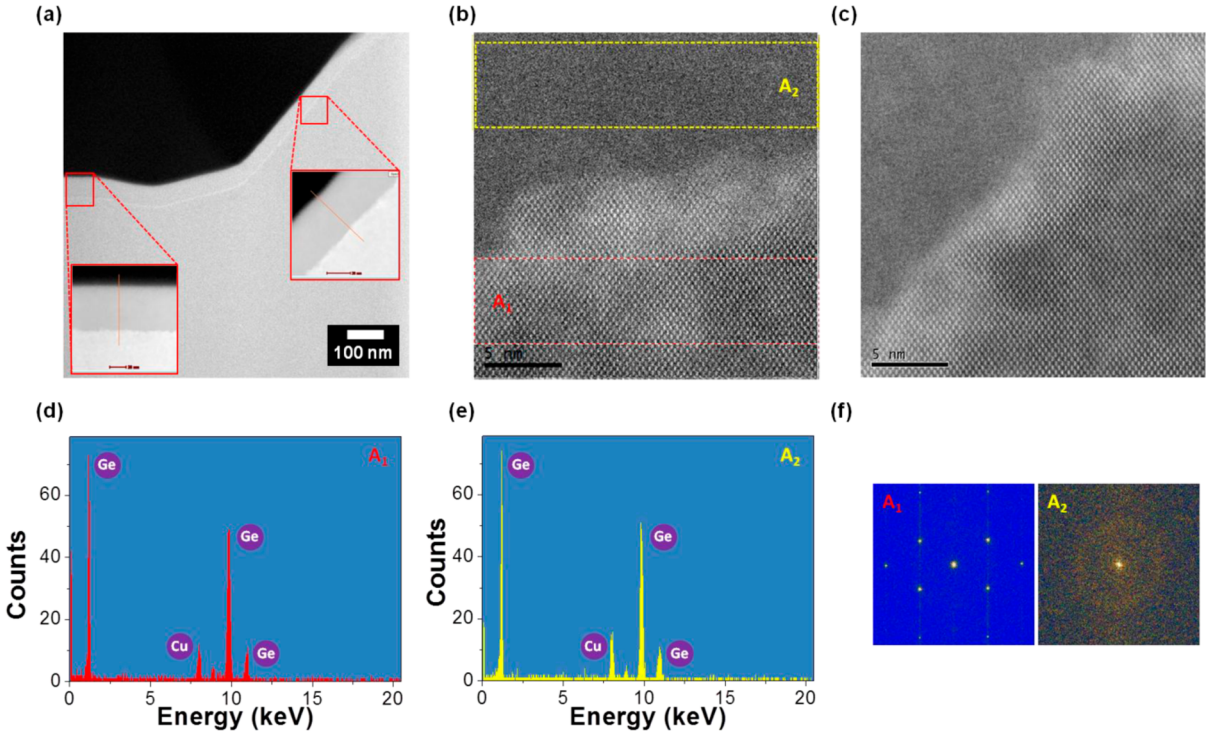

Figure 2. (a) Low-magnification TEM image obtained from both flat regions between i-MacEtch produced Ge pyramids and sidewall of the Ge pyramid. Inset shows HAADF STEM images with a scale bar of 20 nm. (b, c) High-magnification HAADF STEM images obtained from the interface between amorphous and single crystalline area of the flat region and sidewall facet of the pyramid, respectively. (d, e) EDX data taken from single crystalline (A_1) and amorphous region (A_2), respectively; indicating negligible difference in chemical composition. (f) Selective-area FFT images taken from A_1 and A_2 in (b).

nanostructures, produced using an Au mesh pattern (Figure 1d–i) with a diameter and spacing of 400 nm in a mixture of HF (0.56 M), DI water (1.1 M), and $KMnO_4$ (0.16 mM) for 10 min. In this case, a considerably shorter etching time was used which yielded the shallow indentation without clear crystal facets. We believe that inverse micropyramid array with clear crystal facets using such Au mesh catalyst pattern could be formed, as in the case of InGaP/GaAs i-MacEtch,[21] with prolonged etching time and adjusted recipe. The inset shows a zoomed-in SEM image with a scale bar of 500 nm. Diameter and spacing of the formed indentation were measured to be 600 and 200 nm, respectively. The depth of the indentation is 150 nm. This dimension change with respect to the pattern size (*i.e.*, increased diameter and decreased spacing) is a result of lateral etching of Ge underneath the peripheral of the Au mesh. Figure 1d shows a schematic drawing of Au mesh pattern and the illustration of the formation mechanism of the nano-indentation. Similar to the formation of the Ge pyramids (Figure 1b), Ge outside the Au–Ge interface was preferentially etched first because holes were diffused to the off-metal area due to the limited mass transport etching condition used. Lateral etching underneath the Au pattern then followed and the Au mesh was completely peeled off due to the undercut etching.

Mechanism of Ge i-MacEtch. MacEtch process is initiated by holes (h^+) generated from the oxidant on the noble metal surface and subsequently diffused to the semiconductor underneath or around the metal. The mechanism is governed by two main steps: carrier generation and mass transport.[22] The first step generates free carriers (holes) by reduction of the oxidant catalyzed by the metal, and the holes are then consumed by first oxidizing the semiconductor directly under the metal. The mass transport refers to the process where the etching reagent dissolves the oxidized semiconductor along the interface of the metal catalyst and semiconductor. However, if the amount of holes injected to the semiconductor is larger than amount of the holes consumed, the holes are no longer confined under the catalyst, resulting in the diffusion of the holes to outside the metal–semiconductor interface. Since this area is directly exposed to the acidic solution, the oxidized semiconductor outside the metal is etched away. Therefore, the etched area is located between the catalyst pattern and the catalyst remains at the Ge surface instead of descending into the semiconductor, thus it is the so-called I-MacEtch.[19] Limited mass transport plays a critical role in i-MacEtch. The limited mass transport in the case of MacEtch of Ge can be attributed to the strong van der Waal's force between Au and Ge[23] and the higher hole mobility of Ge (see Table S1). This makes hole diffusion to off-metal area in Ge much faster than that of other semiconductor materials.[24]

H_2O_2 is the commonly used oxidant for Si MacEtch. However, it cannot be used for clean MacEtch of Ge because H_2O_2 itself etches Ge without the presence of metal catalysts. Therefore, a weaker oxident, potassium permanganate ($KMnO_4$, 1.51 V), is used as the oxidant in this work because it has a redox potential lower than that of H_2O_2 (1.763 V), as shown in Figure S3.[25] It should be noted that Ge with no metal catalysts present was found to be intact under the same etching conditions for generating the arrays of pyramids and nano-indentation surface patterns shown in Figure 1a,c. This indicates that our etching process is indeed metal-assisted.

We hypothesize that in the HF-$KMnO_4$-H_2O solution, the Ge etching is carried out by the following chemical reactions. $KMnO_4$ generates $MnO4^-$ ions in the aqueous solution, which

DOI: 10.1021/acsnano.8b01848
ACS Nano XXXX, XXX, XXX–XXX

reacts with H^+ to produce holes in the presence of the Au catalyst by eq 1:

$$MnO_4^- + 8H^+ \rightarrow Mn^{2+} + 4H_2O + 5h^+ \quad (1)$$

Holes are injected into the Ge surface, resulting in the formation of amorphous Ge or Ge oxide. Dissolution process of Ge may consist of the combination of direct dissolution of Ge *via* removal of amorphous Ge and formation of Ge oxide followed by dissolution of oxide, which can be described by eqs 2[26,27] and 3, respectively. The formation of amorphous film, composed mostly of Ge, is revealed by STEM as will be shown below. Further study is needed to clarify which process plays a dominant role in i-MacEtch of Ge.

$$\begin{aligned} &Ge + 2h^+ + 2HF = GeF_2 + 2H^+ \\ &2GeF_2 = Ge(\text{amorphous}) + GeF_4 \end{aligned} \quad (2)$$

$$\begin{aligned} &GeF_4 + 2HF = H_2GeF_6 \\ &GeF_2 + 2H_2O = GeO_2 + 2HF + H_2 \\ &GeO_2 + 6HF = H_2GeF_6 + 2H_2O \end{aligned} \quad (3)$$

Structural and Chemical Characterization of the i-MacEtched Surface Structures: STEM and XPS. STEM measurements were carried out to investigate morphology of the etched surface. Figure 2a shows low magnification cross-sectional images obtained from both flat region between i-MacEtch fabricated Ge pyramids and sidewall facet of pyramids. Top layer that follows the surface has different contrast and structure compared to those of bulk Ge substrate. Inset of Figure 2a shows a high-angle annular dark-field (HAADF) STEM image with a scale bar of 20 nm. It is evident that an amorphous layer was formed on top of the c-Ge. The thickness of amorphous layer is estimated to be approximately 50 nm. Figure 2b,c shows HAADF STEM images of the interface between amorphous and c-Ge from the flat region and sidewall facet of the pyramids, respectively. Stoichiometric analysis of the amorphous and single crystalline area was performed by energy dispersive X- ray spectroscopy (EDX) to identify the chemical composition, which is very important for the device performance. Figure 2d,e shows EDX spectra taken from the single crystalline (A_1) and amorphous region (A_2) in Figure 2b, respectively. Ge elements of Ge_L and Ge_K were measured at energy of 0.95, 9.9, and 11 keV, while oxygen was not detected from both A_1 and A_2. EDX confirmed that the amorphous layer was composed purely of Ge. Figure 2f shows fast Fourier transform (FFT) images taken from A_1 and A_2. A halo, more diffused and less obvious circle, from FFT image of A_2 is attributed to randomly oriented nanocrystalline Ge phase inside amorphous matrix. Careful analysis of FFT images indicates that top amorphous Ge layer contains tiny domains, mostly <1 nm, which have short-range ordering atoms.

Figure 3a,b shows XPS spectra obtained from the Ge(3d) and Ge(2p3/2) bonding states of the pyramid Ge sample, respectively. Shoulders were observed from the Ge(3d) and Ge(2p3/2) core level peaks, which indicate the presence of GeO_2 and/or suboxides (GeO_x, $x < 2$). However, the XPS intensity of the shoulders is much weaker, compared to that of native oxide on Ge.[28] This indicates the presence of only small amount of GeO_x. The weak GeO_x peak should be attributed to the fact that the native oxide cannot be easily grown on the amorphous Ge surface.[29] We also note that Ge(2p3/2) core level peak shifts by approximately 0.4 (1217.3−1216.9) eV to

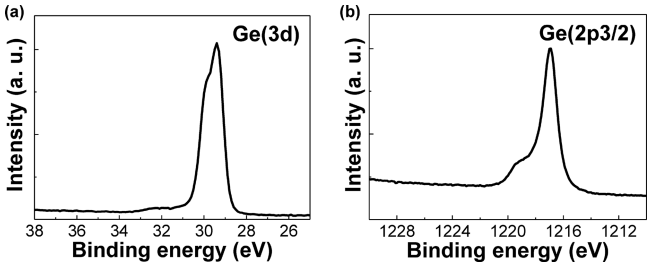

Figure 3. High-resolution XPS showing the (a) Ge(3d) and (b) Ge(2p3/2) bonding states.

the lower energy side, which could be associated with lower oxidation state of amorphous Ge *versus* crystalline Ge.[29] Note that if GeO_x or GeO_2 was produced by MacEtch, it should be removed by DI water and HF because of its high solubility. This proves that the amorphous layer formed at the top surface of the etched sample predominantly consists of Ge itself, which agrees well with the EDX. This amorphous Ge layer plays a critical role in reducing dark current of textured photodiodes, which will be discussed in a later part of this paper.

Optical Characterization of the Textured Ge Surfaces and FDTD Simulations. To evaluate the optical properties of the textured Ge surfaces for the application of optoelectronic devices, reflectance spectrum were obtained. Figure 4 shows the

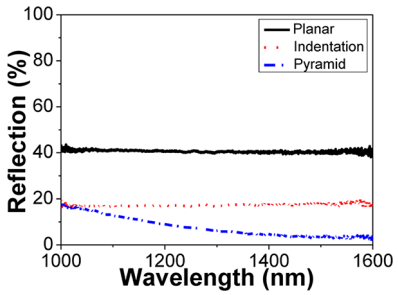

Figure 4. Surface reflection spectrum of planar and textured (*e.g.*, pyramid and nano-indentation) Ge surfaces measured in a wavelength range of 1000−1600 nm.

measured reflection spectra of polished and textured (*i.e.*, pyramid and indented structures) Ge surfaces at a wavelength range of 1000−1600 nm. The polished Ge surface reflected approximately 40% of the incoming light. The measured reflection of the polished Ge agrees well with that of calculated reflection based on the complex-matrix form of the Fresnel equations.[30] In contrast, the reflection for the samples with the indentations was reduced to around 17% across the same wavelength range. The reflection for the pyramid Ge surface was measured to be 17% at the wavelength of 1000 nm and it gradually decreased to 3% as the wavelength approached 1600 nm. The wavelength dependence for the pyramid surface can be explained by resonance (*i.e.*, light multireflection) between adjacent pyramids. However, wavelength dependence for the indentation surface was not observed across the wavelength range. The light multireflection and resonance are not taking effect for the indentation structure due to the relatively smaller dimension compared to the wavelength. In order to investigate the reflection at other wavelength ranges below 1000 nm, we have simulated the reflection using Lumerical finite-difference-time-domain (FDTD) from ultraviolet (UV) to near-infrared (NIR) ranges. Figure S4 shows the simulated reflection of the

DOI: 10.1021/acsnano.8b01848
ACS Nano XXXX, XXX, XXX−XXX

planar and textured Ge surfaces from 200 to 1000 nm. For the micropyramid structure, the spectrum follows that of the planar surface with reduced reflection, originated from the effect of graded refractive index. On the other hand, nano-indented structure indicates a clear photonic crystal effect with a significant reflection drop at 700 nm as the wavelength approaches periodicity of the structure. Overall, the reflection of both micropyramid and nano-indented surfaces is reduced as compared to the planar one at UV, visible, and NIR wavelengths. The clearly improved antireflection properties of the periodically textured Ge surfaces fabricated by i-MacEtch can potentially be applicable for advanced light trapping in Ge-based optoelectronic devices.

To understand how light is trapped in these textured surfaces, simulations were performed by Lumerical FDTD at 1, 1.4, and 1.8 μm, respectively. Planar incident light wave is shined on the surface, and the textures are set to be infinitely periodic for both cases. The absorption improvement compared to planar surface accredits to combined contribution of less direct reflection and absorption enhancement in the convex sphere or pyramid Ge periodic parts. With the introduction of the middle layer between air and bulk Ge, the refractive index distribution change becomes less abrupt and thus results in the suppressed light reflection. For the nano-indented structure, where the dimension is comparable to the wavelength, it can be seen that the light could not form resonance and penetrate inside the indented area. The light trapping effect would be enhanced due to the scattering.[31] In the case of micropyramid patterning, where the structure dimension is much larger than the light wavelength, the multireflection process plays a primary role in absorption enhancement.[31] The steady state of light intensity distributions for the two patterned structures is illustrated in Figure 5.

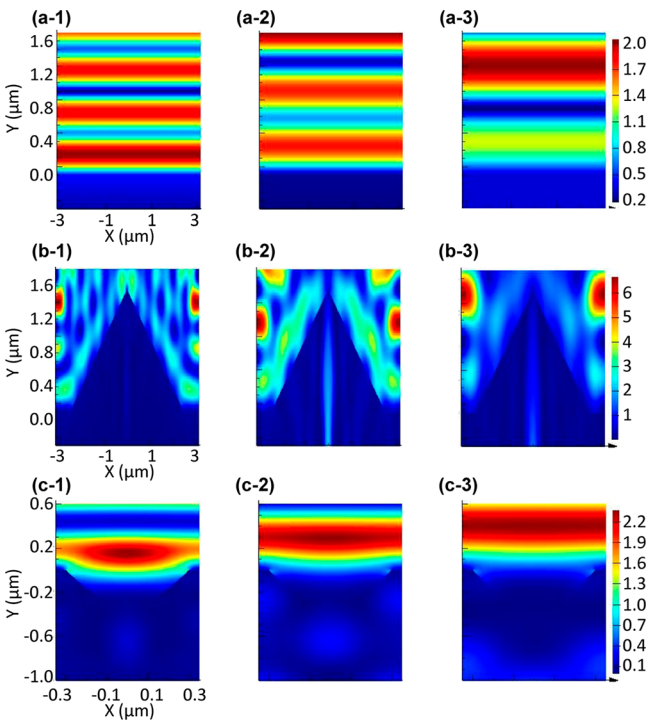

Figure 5. Steady state of light intensity distributions for (a) planar, (b) pyramid, and (c) indentation Ge surfaces at 1 (*e.g.*, a-1), 1.4 (*e.g.*, a-2), and 1.8 (*e.g.*, a-3) μm, respectively.

Results on planar surface are also included for comparison. For the planar surface (Figure 5a), the interference pattern between incident and reflected light wave forms periodic electrical field distribution and the spatial periodicity becomes larger as wavelength increases (Figure 5a-1 to Figure 5a-3). For the indented Ge structure (Figure 5c), as the incident light wavelength varies from 1 to 1.8 μm, the steady-state light intensity location moves upward. For the micropyramid structures (Figure 5b), since the periodicity is more than three times larger than the wavelength scale over the wavelength range from 1 to 1.8 μm, the electric field intensity distribution has several peaks within the valleys between adjacent pyramids. With wavelength shifting to longer wavelength, the number of peaks becomes less. Additionally, due to increased etching depth for the pyramid structure compared to the indented one, there is more chance for the light to be reflected and absorbed by the pyramids until it is reflected upward to air, thus the absorption for the pyramid is more efficient than the indented structure.

Photodiode Characterization. The sensitivity of a photodiode can be evaluated by the spectral responsivity and normalized photocurrent-to-dark current ratio (NPDR). The responsivity is defined by a ratio of the output current (*i.e.*, photo current−dark current) to power of incident light on the device at a specific wavelength. The NPDR is determined by a ratio of the photocurrent to dark current divided by incident light power. A large NPDR indicates suppressed dark current without sacrificing the responsivity. Another important figure of merit of photodiodes is dark current because it is one of the main sources for noise in image sensors. The sensitivity and dark current of our textured photodiodes were characterized and compared to those of photodiodes made on planar surface. Figure 6a shows the measured dark current−voltage (I−V) of

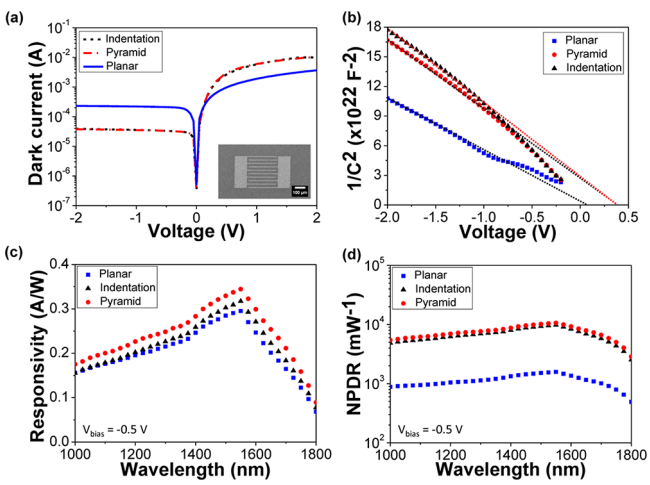

Figure 6. Photodiode characterization: (a, b) Dark current and capacitance of the photodiodes as a function of voltage bias. Inset in Figure 6a is a top SEM image of the fully fabricated photodiode with interdigitated electrodes. (c, d) Responsivity and NPDR of the photodiodes at −0.5 V as a function of wavelength.

three types of photodiodes. The planar diode exhibited a clear rectifying I−V characteristic with an on/off current ratio of 16 at 2/−2 V. Interestingly, dark current of photodiodes fabricated on the pyramid and indented surface was reduced at a negative bias, compared to that of photodiode on the planar surface. We measured dark current of 210, 38.6, and 37.4 μA at a voltage

DOI: 10.1021/acsnano.8b01848
ACS Nano XXXX, XXX, XXX−XXX

bias of −2 V for photodiodes on planar, indented, and pyramid surfaces, respectively. This leads to the on/off current ratio of 259 and 267 of the photodiodes on indented and pyramid surfaces at −2 V, more than an order of magnitude of enhancement.

As shown in the HR-TEM image (Figure 2), the surface of the c-Ge was converted to amorphous as a result of I-MacEtch. Therefore, a thin layer of α-Ge existed between the top Schottky metal electrodes and bottom c-Ge. Enhanced Schottky barrier height (SBH) of α-Ge in contrast to c-Ge was reported and attributed to the increase in the separation between the mobility edges in α-Ge.[32] Oh *et al.*[32] and Ciftcioglu *et al.*[33] inserted α-Ge and α-Si layers between metal electrodes and Ge surface, respectively, to reduce dark current of Ge photodiodes by as much as 2 orders of magnitude. Figure 6b shows a comparison of capacitance−voltage ($1/C^2-V$) of the photodiode structures measured at 1 MHz under dark conditions. The SBH can be determined by the voltage-axis intercept of the $1/C^2-V$ curve. The SBH of the photodiode on planar surface was estimated to be 0.08 eV, while it increased to 0.4 eV for the photodiodes on both indentation and pyramid surfaces. We attribute the increased SBH to the α-Ge layer formed on c-Ge as a result of i-MacEtch. Therefore, our method, which simultaneously forms the textured surface terminated with the α-Ge layer, serves as a monolithic method for reduction in both dark current and surface reflection. Moreover, α-Ge has been demonstrated as an effective passivation layer for Ge solar cells.[34] The self-passivation effect of the α-Ge is another advantage of I-MacEtch technique toward its application for Ge optoelectronic and photonic devices.

Figure 6c,d shows the responsivity and NPDR of photodiodes measured at −0.5 V at a wavelength range from 1000 to 1800 nm. Textured photodiodes exhibit enhanced responsivity and NPDR compared to those of planar photodiodes. Measured responsivity of the planar photodiode was 0.16 A/W at 1000 nm, linearly increasing to 0.30 A/W as the wavelength goes to 1550 nm. Maximum responsivity of 0.30 A/W was measured at 1550 nm, and it sharply dropped to 0.07 A/W at 1800 nm. This trend can be correlated with direct and indirect band gap energies of Ge of 0.67 and 0.81 eV, which correspond to the wavelength of 1850 and 1530 nm, respectively. Similar behavior, but showing larger responsivity, was observed for indented and pyramid photodiodes over the entire wavelength range. Maximum responsivity of 0.30, 0.32, and 0.34 A/W was measured from the planar, indented, and pyramid photodiodes at 1550 nm, respectively. The NPDR of the planar photodiode was in the range of 10^3 mW^{-1}, while that of both indented and pyramid photodiodes is approaching 10^4 mW^{-1}, which is more than 5 times higher than the planar photodiode. This value is higher than those of other Ge photodiodes[35−38] and comparable to the best reported result.[39] To better understand device performance, the band diagram of the Ge Schottky photodiodes with and without the α-Ge layer is presented (see Figure S5). Dark current of the textured photodiode is suppressed by the increased SBH, compared to that of the planar photodiode. At the same time, the α-Ge layer also impedes the collection of photogenerated holes, which leads to suppressed photo current. Therefore, the effect from the increased SBH on responsivity of the photodiode without antireflective surface may not be significant because both dark and photo currents are reduced. However, performance enhancement of the textured Ge photodiodes was demonstrated both in lower dark current and higher responsivity and NPDR with respect to the planar untreated surface. This indicates that the enhanced responsivity and NPDR must be attributed to both the increased SBH and reduced surface reflection of the textured surface.

CONCLUSION

In conclusion, we have reported the formation of textured surface in c-Ge using I-MacEtch and the effect on photodiode performance. Two types of the textured surfaces with arrays of pyramids or nano-indentations have been achieved using periodic Au dot array and an Au mesh pattern, respectively. The mechanism of I-MacEtch of Ge has been investigated chemically and structurally. We have demonstrated that α-Ge is created from c-Ge as a direct result of I-MacEtch. Schottky Ge photodiodes have been realized on the I-MacEtched surfaces, showing enhanced performance including increased responsivity and NPDR, and reduced dark current, compared to the planar counterpart. The dark characteristics improvement was attributed to increased SBH and self-passivation associated with α-Ge, and the light characteristics enhancement was confirmed to be the result of antireflection due to surface textures. This study established a monolithic integration path that is enabled by the facile I-MacEtch method to form not only the amorphous layer for enhanced electrical performance but also textured surfaces for efficient light management simultaneously. Further studies will include optimizing the thickness of the amorphous layer and surface texture pattern with respect to the desired wavelength range. The outcome will provide great potentials toward high-performance Ge-based optoelectronic devices and other semiconductors in general using the simple and powerful I-MacEtch technology.

EXPERIMENTAL SECTION

Formation of Textured Surfaces using i-MacEtch. The processing began with a thorough cleaning of unintentionally doped c-Ge wafer (Wafer World, Inc. resistivity >40 Ω·cm) with acetone, IPA, and DI water. For pyramid shaped nanostructures, the Ge substrate was first photo lithographically patterned with an array of dots. The samples were dipped in 10:1 buffered oxide etch (BOE) for 10 s to remove native oxide and immediately loaded into CHA SEC-600 e-beam evaporator. Twenty-five nm of Au catalyst was e-beam evaporated with a deposition rate of 0.2 Å/s and lifted off. For indentation shaped nanostructures, nanosphere lithography (NSL) technique was used to form planar ordered arrays of polystyrene spheres. A polystyrene bead solution prepared by the standard recipe[40] was spin-coated on Ge samples. The spin-coating process consisted of three steps: (i) 330 rpm for 8 s (to spread the beads solution evenly); (ii) 300 rpm for 20 s (to spin away the excess bead solution); (iii) 1700 rpm for 8 s (to spin off the excess materials from the edges). The diameter of the polystyrene bead was reduced to 400 nm by a RIE etcher (Diener) with 2 sccm of oxygen at RF power of 500 W and a pressure of 150 mTorr for 8 min. Twenty-five nm-thick Au was deposited on the samples and lifted off by sonicating the samples in IPA. The Ge samples with the Au film were etched in a solution of 49% HF, DI water, and $KMnO_4$, the oxidant. A magnetic stir bar was used to completely dissolve $KMnO_4$ in HF. The array of micropyramids for the device was formed on the Ge surface by etching in the mixture of $KMnO_4$ (0.32 mM), HF (0.56 M), and DI water (1.1 M) for 90 min. Similarly, nano-indentation was realized by the mixture of $KMnO_4$ (0.16 mM), HF (0.28 M), and DI water (0.55 M) for 10 min. Etched samples were rinsed in DI water and dried by nitrogen blow.

Characterizations of the i-MacEtched Surface Structures. The top and tilted views of the etched samples were inspected with scanning electron microscopy (SEM, Hitachi S-4700). X-ray photo-

DOI: 10.1021/acsnano.8b01848
ACS Nano XXXX, XXX, XXX−XXX

electron spectroscopy (XPS, Kratos Axis ULTRA) measurements were carried out on planar and etched Ge surface to analyze the chemical composition of the amorphous layer formed on the etched surface. The surface reflection of the Ge pyramid and indentation were measured using a custom-built reflection system over the spectral range from 1000 to 1600 nm at room temperature. Detailed measurement setup was described in elsewhere.[41] The size of the beam spot was approximately 300 × 300 μm^2. The surface reflection of a control sample (*i.e.*, planar Ge) was also measured to compare with that of the textured samples.

Scanning Transmission Electron Microscope (STEM). STEM measurements were performed on a FEI Titan 80−200 electron microscope operated at 200 kV and configured with a CEOS probe aberration corrector, which allowed us to achieve a resolution of 0.8 Å at 24.5 mrad convergence angle, and 20 pA probe current, measured using the calibrated response of a Gatan US1000 CCD camera (Gatan, Pleasanton, CA). By using STEM detector collection angles of 54−270 mrad, the image intensity scales as Z^{α}, where α is in the range of 1.6−1.9 and Z is the atomic number of the atoms of analyzing column. The FEI Titan was equipped with an EDAX X-ray spectrometer (Ametek, Inc., Berwyn, PA, model PV97-61850 ME, active area 30 mm^2, collection angle ∼0.09 srad), and the sample rod was rotated to +17° to maximize X-ray signal collected by the EDX spectrometer. X-ray energy dispersive spectroscopy (EDS) with energy resolution of 132 eV per channel is used to gain composition information about materials.

Fabrication and Characterization of Vertical Schottky Ge Photodiodes. Vertical Schottky Ge photodiodes were fabricated on planar and i-MacEtch textured Ge surfaces. Schottky interdigitated metal electrodes (Ti/Au = 5/75 nm) were deposited on the top surface of the planar and textured Ge samples. The electrode fingers had an 8 μm width, 26 μm spacing, and 290 μm length, as shown in Figure 6a inset. Ohmic metal contacts were made on the back side of the Ge substrates with Ti/Au of 5/75 nm. Current−voltage (I−V) and capacitance−voltage ($1/C^2$−V) characteristics of the photodiodes were measured using a semiconductor parameter analyzer (Keithley 4200 SCS). Photocurrent was measured using a chopper and a lock-in amplifier (SR850, Stanford Research Systems). Tungsten-halogen lamp (ASBN-W, Spectral Products) was used as a light source and monochromator with a slit width of 500 μm to control the wavelength of light from 1 to 1.8 μm with a step of 0.5 μm. We used two lenses to focus and control the beam size to ensure that the output beam covers the whole area of the fabricated Ge photodiodes. Light power of each wavelength was carefully measured by a power meter (S132C, Thorlabs).

ASSOCIATED CONTENT

Supporting Information

The Supporting Information is available free of charge on the ACS Publications website at DOI: 10.1021/acsnano.8b01848.

SEM images showing hole diffusion to off-metal area in Ge, SEM images of Ge pyramid during MacEtch, comparison of Ge band edge energies, the MnO_4^{2-}/Mn^{2+}, and H_2O_2/H_2O redox potential, simulated reflection of planar and textured Ge surfaces at a wavelength range of 200−1000 nm, energy band diagrams of Ge Schottky photodiodes with and without α-Ge layers, comparison of hole mobility and diffusion coefficient of Ge with other semiconductors (PDF)

AUTHOR INFORMATION

Corresponding Author

*E-mail: xiuling@illinois.edu.

ORCID

Munho Kim: 0000-0002-0379-1886
Xin Yin: 0000-0002-4759-0226
Jun Li: 0000-0002-7498-6736
Xudong Wang: 0000-0002-9762-6792
Zhenqiang Ma: 0000-0001-9214-1342

Notes

The authors declare no competing financial interest.

ACKNOWLEDGMENTS

This material is based upon work supported by the National Science Foundation under grant no. 14-62946 (fabrication), the U.S. Department of Energy, Office of Basic Energy Sciences, Division of Materials Sciences and Engineering under award no. DE-FG0207ER46471 (device design and characterization), and a gift from Lam Research Corporation (materials).

REFERENCES

(1) Campbell, P.; Green, M. A. Light Trapping Properties of Pyramidally Textured Surfaces. *J. Appl. Phys.* **1987**, *62*, 243.
(2) Garnett, E.; Yang, P. Light Trapping in Silicon Nanowire Solar Cells. *Nano Lett.* **2010**, *10*, 1082−1087.
(3) Yu, Z.; Raman, A.; Fan, S. Fundamental Limit of Nanophotonic Light Trapping in Solar Cells. *Proc. Natl. Acad. Sci. U. S. A.* **2010**, *107*, 17491−17496.
(4) Oh, J.; Yuan, H.-C.; Branz, H. M. An 18.2%-efficient Black-silicon Solar Cell Achieved through Control of Carrier Recombination in Nanostructures. *Nat. Nanotechnol.* **2012**, *7*, 743−748.
(5) Juntunen, M. A.; Heinonen, J.; Vahanissi, V.; Repo, P.; Valluru, D.; Savin, H. Near-unity Quantum Efficiency of Broadband Black Silicon Photodiodes with an Induced Junction. *Nat. Photonics* **2016**, *10*, 777−781.
(6) Otto, M.; Kroll, M.; Kasebier, T.; Salzer, R.; Tunnermann, A.; Wehrspohn, B. Extremely Low Surface Recombination Velocities in Black Silicon Passivated by Atomic Layer Deposition. *Appl. Phys. Lett.* **2012**, *100*, 191603.
(7) Leem, J. W.; Kim, Y. P.; Yu, J. S. Tunable Behavior of Reflectance Minima in Periodic Ge Submicron Grating Structures. *J. Opt. Soc. Am. B* **2012**, *29*, 357−362.
(8) Leem, J. W.; Song, Y. M.; Yu, J. S. Broadband Antireflective Germanium Surfaces Based on Subwavelength Structures for Photovoltaic Cell Applications. *Opt. Express* **2011**, *19*, 26308−26317.
(9) Boyd, D. A.; Frantz, J. A.; Nimalan, R.; Busse, L. E.; Kim, W.; Bayya, S. S.; Sanghera, J. S. Periodically Patterned Germanium Surfaces Modified to Form Superhydrophobic, IR-transmissive Substrates. *Opt. Mater. Express* **2016**, *6*, 3254−3261.
(10) Lu, R.; Ge, C.-W.; Zou, Y.-F.; Zheng, K.; Wang, D.-D.; Zhang, T.-F.; Luo, L.-B. A Localized Surface Plasmon Resonance and Light Confinement-enhanced Near-infrared Light Photodetector. *Laser Photonics Rev.* **2016**, *10*, 595−602.
(11) Lee, S.; Choo, H.; Kim, C.; Oh, E.; Seo, D.; Lim, S. Metal-Assisted Chemical Etching of Ge Surface and its Effect on Photovoltaic Devices. *Appl. Surf. Sci.* **2016**, *371*, 129−138.
(12) Hildreth, O. J.; Lin, W.; Wong, C. P. Effect of Catalyst Shape and Etchant Composition on Etching Direction in Metal-Assisted Chemical Etching of Silicon to Fabricate 3D Nanostructures. *ACS Nano* **2009**, *3*, 4033−4042.
(13) Kim, J.; Kim, Y. H.; Choi, S.-H.; Lee, W. Curved Silicon Nanowires with Ribbon-like Cross Sections by Metal-Assisted Chemical Etching. *ACS Nano* **2011**, *5*, 5242−5248.
(14) Kong, L.; Song, Y.; Kim, J. D.; Yu, L.; Wasserman, D.; Chim, W. K.; Chiam, S. Y.; Li, X. Damage-Free Smooth-Sidewall InGaAs Nanopillar Array by Metal-Assisted Chemical Etching. *ACS Nano* **2017**, *11*, 10193−10205.
(15) Mohseni, P. K.; Kim, S. H.; Zhao, X.; Balasundaram, K.; Kim, J. D.; Pan, L.; Rogers, J. A.; Coleman, J. J.; Li, X. GaAs Pillar Array-based Light Emitting Diodes Fabricated by Metal-Assisted Chemical Etching. *J. Appl. Phys.* **2013**, *114*, 064909.
(16) Song, Y.; Mohseni, P. K.; Kim, S. H.; Shin, J. C.; Ishihara, T.; Adesida, I.; Li, X. Ultra-high Aspect Ratio InP Junctionless FinFETs by

DOI: 10.1021/acsnano.8b01848
ACS Nano XXXX, XXX, XXX−XXX

a Novel Wet Etching Method. *IEEE Electron Device Lett.* **2016**, *37*, 970−973.
(17) Shin, J. C.; Chanda, D.; Chern, W.; Yu, K. J.; Rogers, J. A.; Li, X. Experimental Study of Design Parameters in Silicon Micropillar Array Solar Cells Produced by Soft Lithography and Metal-Assisted Chemical Etching. *IEEE J. Photovolt.* **2012**, *2*, 129−133.
(18) DeJarld, M.; Shin, J. C.; Chern, W.; Chanda, D.; Balasundaram, K.; Rogers, J. A.; Li, X. Formation of High Aspect Ratio GaAs Nanostructures with Metal-Assisted Chemical Etching. *Nano Lett.* **2011**, *11*, 5259−5263.
(19) Kim, S. H.; Mohseni, P. K.; Song, Y.; Ishihara, T.; Li, X. Inverse Metal-Assisted Chemical Etching of InP Produces Smooth High Aspect Ratio Nanostructures. *Nano Lett.* **2015**, *15*, 641−648.
(20) Kim, J.; Oh, J. Formation of GaP Nanocones and Micro-mesas by Metal-Assisted Chemical Etching. *Phys. Chem. Chem. Phys.* **2016**, *18*, 3402−3408.
(21) Wilhelm, T. S.; Soule, C. W.; Baboli, M. A.; O'Connell, C. J.; Mohseni, P. K. Fabrication of Suspended III-V Nanofoils by Inverse Metal-Assisted Chemical Etching of $In_{0.49}Ga_{0.51}P$/GaAs Heteroepitaxial Films. *ACS Appl. Mater. Interfaces* **2018**, *10*, 2058−2066.
(22) Kim, J. D.; Mohseni, P. K.; Balasundaram, K.; Ranganathan, S.; Pachamuthu, J.; Coleman, J. J.; Li, X. Scaling the Aspect Ratio of Nanoscale Closely Packed Silicon Vias by MacEtch: Kinetics of Carrier Generation and Mass Transport. *Adv. Funct. Mater.* **2017**, *27*, 1605614.
(23) Buckley, D. H. Adhesion and Friction Behavior of Group IV Elements Germanium, Silicon, Tin, and Lead. *NASA Technical Note (NASA TN D-7930)*; Lewis Research Center, NASA: Cleveland, OH, 1975.
(24) Sze, S. M.; Ng, K. K. *Physics of Semiconductor Devices*; John Wiley & Sons, Inc.: Hoboken, NJ, 2007.
(25) Peng, K. Q.; Hu, J. J.; Yan, Y. J.; We, Y.; Fang, H.; Xu, Y.; Lee, S. T.; Zhu, J. Fabrication of Single-Crystalline Silicon Nanowires by Scratching a Silicon Surface with Catalytic Metal Particles. *Adv. Funct. Mater.* **2005**, *16*, 387−394.
(26) Eddowes, M. J. Anodic Dissolution of P- and N-type Silicon Kinetic Study of the Chemical Mechanism. *J. Electroanal. Chem. Interfacial Electrochem.* **1990**, *280*, 297−311.
(27) Jo, S. K. Surface Reaction of Atomic Hydrogen with Ge(100) in Comparison with Si(100). *Appl. Sci. Convergence Technol.* **2017**, *26*, 174−178.
(28) Onsia, B.; Conard, T.; De Gendt, S.; Heyns, M.; Hoflijk, I.; Mertens, P.; Meuris, M.; Raskin, G.; Sioncke, S.; Teerlinck, I.; Theuwis, A.; Van Steenbergen, J.; Vinckier, C. A Study of the Influence of Typical Wet Chemical Treatments on the Germanium Wafer Surface. *Solid State Phenom.* **2005**, *103*−*104*, 27−30.
(29) Helms, C. R.; Spicer, W. E.; Pereskokov, V. Observation of Strong Bulk Oxidation Effects in Amorphous Germanium by Ultraviolet Reflectance Spectroscopy. *Appl. Phys. Lett.* **1974**, *24*, 318.
(30) See http://www.filmetrics.com/reflectance-calculator for surface reflection of Ge.
(31) Li, J.; Yu, H.; Li, Y.; Wang, F.; Yang, M.; Wong, S. M. Low Aspect-ratio Hemispherical Nanopit Surface Texturing for Enhancing Light Absorption in Crystalline Si Thin Film-based Solar Cells. *Appl. Phys. Lett.* **2011**, *98*, 021905.
(32) Oh, J.; Banerjee, S. K.; Campbell, J. C.; et al. Metal-Germanium-Metal Photodetectors on Heteroepitaxial Ge-on-Si With Amorphous Ge Schottky Barrier Enhancement Layers. *IEEE Photonics Technol. Lett.* **2004**, *16*, 581−583.
(33) Ciftcioglu, B.; Zhang, J.; Sobolewski, R.; Wu, H. An 850-nm Normal-Incidence Germanium Metal-Semiconductor-Metal Photodetector with 13-GHz Bandwidth and 8-μA Dark Current. *IEEE Photonics Technol. Lett.* **2010**, *22*, 1850−1852.
(34) Wu, C.-H.; Hsu, C.-A.; Yang, C.-C. Amorphous Ge Passivation Effects on Ge Solar Cells. *IEEE J. Photovolt.* **2014**, *4*, 968−971.
(35) Chen, L.; Dong, P.; Lipson, M. High Performance Germanium Photodetectors Integrated on Submicron Silicon Waveguides by Low Temperature Wafer Bonding. *Opt. Express* **2008**, *16*, 11513−11518.
(36) Zang, H.-J.; Kim, G.-S.; Park, G.-J.; Choi, Y.-S.; Yu, H.-Y. Asymmetrically Contacted Germanium Photodiode Using a Metal-interlayer-semiconductor-metal structure for Extremely Large Dark Current Suppression. *Opt. Lett.* **2016**, *41*, 3686−3689.
(37) Kim, M.; Seo, J.-H.; Yu, Z.; Zhou, W.; Ma, Z. Flexible Germanium Nanomembrane Metal-semiconductor-metal Photodiodes. *Appl. Phys. Lett.* **2016**, *109*, 051105.
(38) Kim, M.; Liu, S.-C.; Kim, T. J.; Lee, J.; Seo, J.-H.; Zhou, W.; Ma, Z. Light Absorption Enhancement in Ge Nanomembrane and its Optoelectronic Application. *Opt. Express* **2016**, *24*, 16894−16903.
(39) Xia, Z.; Song, H.; Kim, M.; Zhou, M.; Chang, T.-H.; Liu, D.; Yin, X.; Xiong, K.; Mi, H.; Wang, X.; Xia, F.; Yu, Z.; Ma, Z.; Gan, Q. Single-crystalline Germanium Nanomembrane Photodetectors on Foreign Nanocavities. *Sci. Adv.* **2017**, *3*, e1602783.
(40) Cheung, C. L.; Nikolic, R. J.; Reinhardt, C. E.; Wang, T. F. Fabrication of Nanopillars by Nanosphere Lithography. *Nanotechnology* **2006**, *17*, 1339−1343.
(41) Kim, M.; Seo, J.-H.; Zhao, D.; Liu, S.-C.; Kim, K.; Lim, K.; Zhou, W.; Waks, E.; Ma, Z. Transferrable Single Crystalline 4H-SiC Nanomembranes. *J. Mater. Chem. C* **2017**, *5*, 264−268.

DOI: 10.1021/acsnano.8b01848
ACS Nano XXXX, XXX, XXX−XXX